In situ calibration of the KM3NeT/ARCA neutrino telescope using atmospheric muons

Thesis

submitted in partial fulfillment of the
requirements for the degree of

Bachelor of Science
in
Physics

Author: Jasper Bootsma
Student ID: 1669141
Supervisor: Dorothea Samtleben
2^{nd} corrector: Wolfgang Löffler

Leiden, The Netherlands, June 19, 2020

In situ calibration of the KM3NeT/ARCA neutrino telescope using atmospheric muons

Jasper Bootsma

June 19, 2020

Abstract

KM3NeT is an international collaboration currently working on the construction of a neutrino detector in the Mediterranean Sea. During the period evaluated in this research, two detection strings were deployed and active. With this new detector, the KM3NeT collaboration aims to discover the neutrino mass ordering and scan for cosmic neutrino sources. In order to accurately reconstruct neutrino interactions, the detector elements must be synchronized within nanoseconds.

The goal of this research is to evaluate whether the signal of passing atmospheric muons can contribute in the time calibration. The data was scrutinized for detector malfunctions and cleaned. The detector performance was then checked by using signal coincidences between detector elements to evaluate correlated signals, stemming from atmospheric muons. This allowed also to determine the dependence of the muon rate on the depth and assess potential time offsets. A time offset of 30 ns between the two operating detector strings was found, which will require further investigations.

Acknowledgements

I would like to thank Dorothea Samtleben for her supervisory guiding, Lodewijk Nauta and Karel Melis for all their help with the coding and answering my daily questions, and the entire KM3NeT group at Nikhef for the “gezelligheid” in general.

Contents

Chapter 1

Introduction

1.1 KM3NeT

This research has been done in collaboration with the KM3NeT group at Nikhef located in Amsterdam. KM3NeT is an international collaboration working on the construction of a new neutrino detector in the Mediterranean Sea. The collaboration is building on the work done using the previous generation of European deep sea neutrino detectors: ANTARES, NEMO and NESTOR. The KM3NeT collaboration will be searching for cosmic neutrino sources with one part of the detector, called ARCA, and aims to discover the neutrino mass ordering using another part, called ORCA. These research goals are elaborated further in section 1.1.1. The mentioned parts of the detector are three-dimensional structures with sensitive light detectors. The interactions of neutrinos with the seawater will be detected through the detection of Cherenkov radiation produced by charged particles created in these neutrino interactions. Cherenkov radiation and the processes in the neutrino interactions are explained in sections 1.4.1 and 1.2, respectively.

Once completed, the total volume of this new generation detector will exceed one cubic kilometer, hence its name **KM**^{3} **Ne***(utrino)* **T***(elescope)*. This volume is built from three so called building blocks, with each building block containing 115 Detection Units (DUs).

Currently two of these building blocks are under construction. One off the coast of France at a depth of roughly 2200 to 2400 m, which is called Oscillation Research with Cosmics in the Abyss, or ORCA for short. The other one off the coast of Italy at a depth of roughly 2750 to 3400 m, which is called Astroparticle Research with Cosmics in the Abyss, or ARCA for short. The third will also be off the Italian coast as a part of ARCA. In a possible next phase more building blocks will be added to ARCA on a Greek site [1].

ORCA and ARCA are both built from the same elements. As mentioned, both detectors consist of 115 DUs, in which every DU is a construction of two ropes anchored in the seabed, held vertical by two buoys at the top. Every DU has 18 Digital Optical Modules (DOMs) attached to it at regular intervals. Every Digital Optical Module in its turn contains 31 Photomultiplier Tubes (PMTs). Schematic depictions of both a DU and a DOM are shown in figures 1.1 and 1.2, respectively. The contents of a DOM will be elaborated further in section 1.4.

However, since the research goal of the two detectors is different, so are their

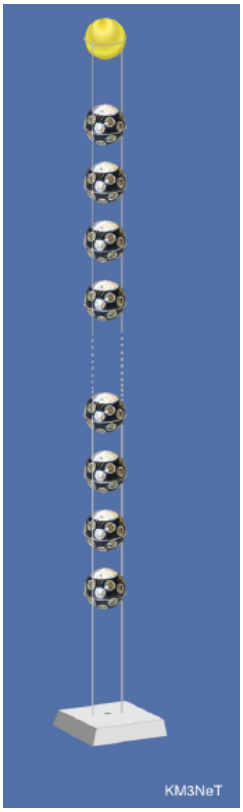

Figure 1.1: Schematic depiction of a DU, with DOMs suspended between two lines held vertical by a buoy [1].

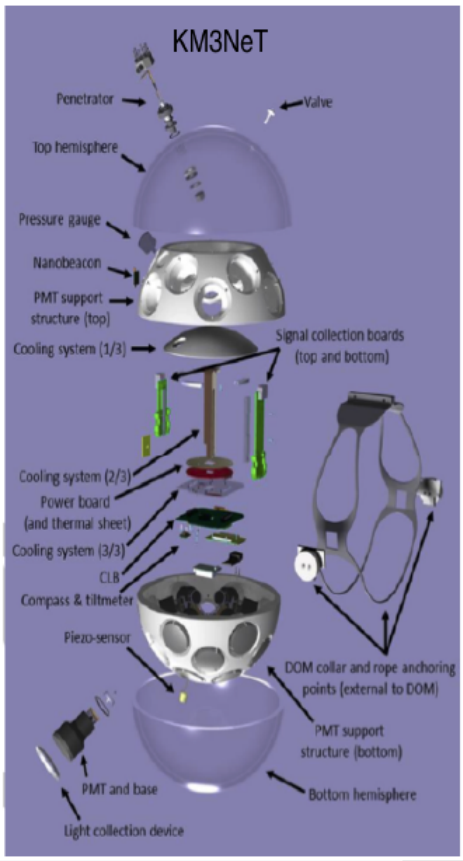

Figure 1.2: Exploded view of a DOM [1].

physical dimensions. ORCA is designed for detecting neutrinos at lower energies and is therefore smaller with two DUs being roughly 20 meters apart and two DOMs on the same DU 9 meters apart. ARCA on the other hand is designed to detect high energy cosmic neutrinos. To achieve this, it is a lot bigger with a distance of about 95 meters between two DUs and an elevation of roughly 36 meters between two DOMs [1].

1.1.1 KM3NeT research goals

The high energy neutrinos ARCA is aiming to detect are theorized to come from the most energetic places in the universe, which can not only (or even not at all) be seen in optical light. Over the last century the means have been created to see the universe not only in optical light, but over the full spectrum of electromagnetic waves. For more than 50 years the skies were scanned with only telescopes for this traditional medium. However, since the first detection of cosmic neutrinos by IceCube in 2013 [2] and the first detection of gravitational waves by LIGO in 2015 [3] we can not only "see" the universe, but also "feel" and "hear" it.

Using all these "senses" together is called multi-messenger astronomy and it will be both used and aided by ARCA. Used because an observation in the electromagnetic spectrum (or one of gravitational waves) is necessary to confirm a neutrino

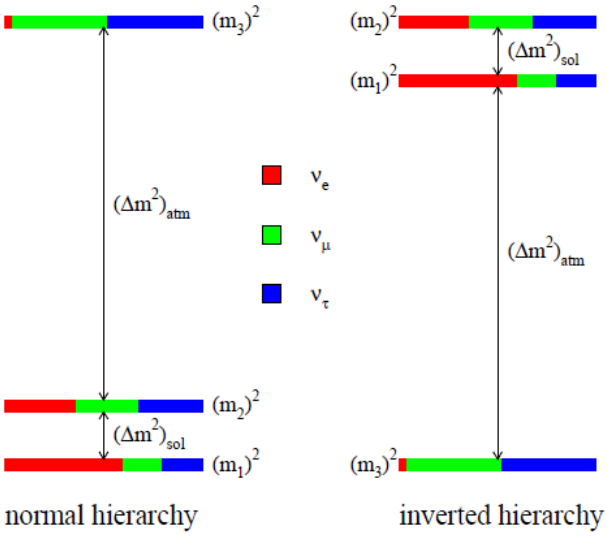

Figure 1.3: Cartoon of the normal and inverted neutrino mass ordering. The colors indicate the fractions of the flavor mixing for each mass [4].

source. Aided because the neutrino's little interaction (in the source and interstellar medium up until detection) means ARCA could give insight into the interior of the source that could not be attained through the use of the traditional electromagnetic medium. Last but not least ARCA will complement IceCube to give full sky coverage for neutrino telescopy and a better view on the galactic plane.

The research goal for ORCA is to discover the neutrino mass ordering (NMO). According to our current knowledge of the Standard Model of Elementary Particles (SM) neutrinos have three flavor eigenstates: ν_e, ν_μ and ν_τ (electron neutrino, muon neutrino and tau neutrino, respectively). In previous experiments it has been established that a neutrino produced in one eigenstate can be detected in another eigenstate [5, 6, 7, 8]. The only consistent conclusion from these results is "neutrino mass-induced flavor oscillation." This implies that neutrinos are not massless and that the mass eigenstates (ν_1, ν_2, ν_3) are different from the flavor eigenstates (ν_e, ν_μ, ν_τ) [4]. The mass and flavor eigenstates are mixed, which means that there is no such thing as an "electron neutrino mass", "muon neutrino mass" or "tau neutrino mass", but merely a low, middle and high mass. To relate the elements of the mixing matrix to experimental observables, an "ordering" of the neutrino masses is required. This order is defined so that $m_2^2 > m_1^2$ and $\Delta m_{21}^2 < \left|\Delta m_{31}^2\right|$.[1] This means that the sign of $\left|\Delta m_{31}^2\right|$ defines the characterization of the neutrino mass ordering [4]. Both normal and inversed ordering are depicted in figure 1.3, to give a visual representation of the flavor mixing in the mass eigenstates.

Uncovering the ordering of these neutrino mass eigenstates could assist other research fields to make progress, NMO is for example a prerequisite to unambiguously measure leptonic violations of charge-parity symmetry [9]. Some other fields that have to gain from the determination of the NMO are the search for neutrinoless double-β decay [10], distinguishing the (Dirac or Majorana) nature of neutrinos and the determination of the absolute neutrino masses.

[1] Here m_i is the observable of the mass eigenstate ν_i and Δm_{ij} is the mass difference between the observables of mass eigenstates ν_i and ν_j.

1.2 Neutrino interaction

Due to their different research goals ORCA and ARCA are optimized for different neutrino energy ranges. ORCA is sensitive for the low energy atmospheric neutrinos and ARCA for the high energy cosmic neutrinos.

The cosmic neutrinos researched in ARCA originate directly from high energetic interactions in a massive object out in the universe, such as quasars and gamma-ray bursts. The atmospheric neutrinos researched in ORCA, however, are created in our own atmosphere. As cosmic rays bombard the earth, they create so called showers in the atmosphere where many particles are created and decay. Some of these created particles are mesons, combinations of a quark and an antiquark. The interesting mesons in question are charged kaons and pions, since both of them most often (with branching ratios[2] of roughly 63.55% and just short of 100%[3], respectively) leptonically decay to a muon - muon neutrino pair. Which of the two is an antiparticle of course depends on the charge of the original particle. The most common decays (apart from the sign of the charge) of kaons and pion therefore are:

$$\mathrm{K}^+ \rightarrow \mu^+ + \nu_\mu \tag{1.1}$$

and

$$\pi^- \rightarrow \mu^- + \overline{\nu_\mu} \tag{1.2}$$

Here K^+ is a positively charged kaon, π^- is a negatively charged pion, μ^- (μ^+) is an (anti)muon and ν_μ ($\overline{\nu_\mu}$) is a muon (anti)neutrino.

Kaons can also hadronically decay (which means they decay with only hadrons as products) into a set of charged and/or neutral pions, of which the charged pions will then decay into the muon and muon neutrino. For example (the most common hadronic kaon decay, with a branching ratio of 20.66%) as following:

$$\mathrm{K}^+ \rightarrow \pi^+ + \pi^0 \rightarrow \mu^+ + \nu_\mu + 2\gamma \tag{1.3}$$

Where π^0 is a neutral pion, which most commonly decays into two photons represented by the 2γ.

Both these cosmic and atmospheric neutrinos will then travel through the earth. Once in the seawater on the other side of the globe, the neutrinos have to interact in

[2]The branching ratio of a decay form is the chance that the decay taking place will happen through that type of decay.

[3]A pion has as sole other decay type: a decay into an electron - electron neutrino pair, which has a branching ratio of 0.0123%.

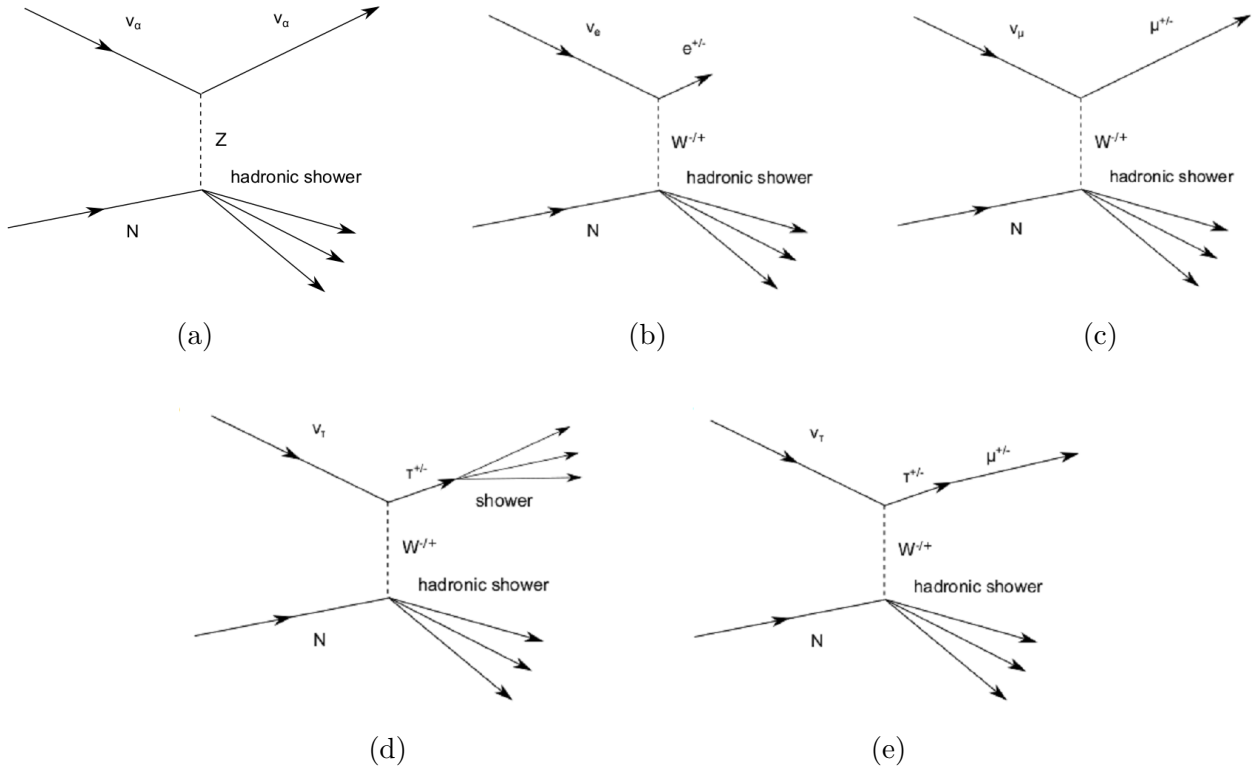

Figure 1.4: Feynman diagrams of neutrino interactions with detectable products through Neutral Current in (a) and Charged Current in (b), (c), (d) and (e) [11].

order to create particles that can emit Cherenkov radiation (which will be explained in section 1.4.1). These interactions can happen in two ways: through Neutral Current (NC) and through Charged Current (CC) interactions.

In NC interactions the neutrino transfers a portion of its energy to a nucleon through the (neutral) Z boson, after which the neutrino continues as a neutrino. The extra energy in the nucleon leads to a hadronic shower, a visualization of this can be seen in figure 1.4a. NC interactions look the same for all neutrino flavors.

In CC interactions the previously mentioned portion of energy is transferred through a (charged) W^+/W^- boson, in which case the neutrino ceases to exist and a charged lepton is created. Whereas NC interactions look the same for all neutrino flavors, in CC interactions every flavor is identifiable through the outcome. All flavors have a hadronic shower as an outcome, but the effects of the charged lepton give them their own signature.

The electron (figure 1.4b) has a short mean free path in the seawater, which means it interacts heavily with all the charged particles around it, which results in an electromagnetic shower. In combination with the hadronic shower the result looks like a single shower, comparable to the outcome of NC interactions.

The muon (figure 1.4c) has a much longer mean free path due to its higher mass, which results in less interactions with the seawater. The muon therefore does not create a shower, but a track with its starting point at the same location as the origin of the hadronic shower.

The tau of course has an even longer mean free path, but it also has a very short lifetime of 290.6×10^{-15} s, which is seven orders of magnitude smaller than the

lifetime of a muon of 219.7×10^{-8} s. Although the lifetime of the tau is incredibly short, with high enough energy it will still travel some distance due to its relativistic speed. Taking into consideration that the height of ARCA is roughly 700 m, one can see in figure 2.1 that the tau also decays inside the detector as long as its energy is below 10 PeV (10^7 GeV).

The decay of a tau can happen in many ways, approximately 64.79% of the decay types are hadronic decays in most of which at least one charged pion is created. This charged pion can then either decay into a muon or an electron, as previously discussed.

A tau can also leptonically decay into a tau (anti)neutrino and either an electron - electron neutrino pair or a muon - muon neutrino pair as seen below (which of these particles are antiparticles of course, again, depends on the charge of the original particle).

$$\tau^- \rightarrow \nu_\tau + e^- + \overline{\nu_e} \tag{1.4}$$

and

$$\tau^- \rightarrow \nu_\tau + \mu^- + \overline{\nu_\mu} \tag{1.5}$$

The branching ratios for these decays are 17.82% and 17.39%, respectively.

In the cases where an electron is the resulting charged lepton, the electron will cause an electromagnetic shower which results in a double shower signature as can be seen in figure 1.4d. When a muon is the resulting particle, the muon will create a track. The result will then be a shower and track signature as can be seen in figure 1.4e. In this decay, however, contrary to the decay of a muon neutrino, the starting point of the track is not in the origin of the shower [11].

1.3 Background sources

Besides the signal with a neutrino origin there are some other sources that produce photons, which will be detected and therefore create a background. The main sources of the background radiation detected in KM3NeT are the decay of ^{40}K, bioluminescence and atmospheric muons.

^{40}K is a long-lived isotope of potassium, with a half-life of 1.248×10^9 years. While this isotope makes up only a fraction of all potassium on earth, it is still found in sufficient abundance in both the seawater (in the sea salt) and the glass shell of the DOMs to create a signal. Due to the combination of this abundance and the long half life this phenomenon is responsible for a very constant signal over both space and time.

The decay of ^{40}K can happen through all forms of beta decay. The most common form of decay for ^{40}K, with a branching ratio of almost 90%, is electron emission. In this type of decay calcium (^{40}Ca) is the decay product:

$$^{40}\mathrm{K} \rightarrow {}^{40}\mathrm{Ca} + e^- + \overline{\nu_e} \tag{1.6}$$

Where e^- is an electron and $\overline{\nu_e}$ is an electron antineutrino. The emitted electron can emit Cherenkov radiation (as will be explained in section 1.4.1). This radiation can be detected by multiple PMTs on a nearby DOM and can in this way create a signal (as will be explained in section 1.4.2).

The other manners of decay, with a combined branching ratio of about 10%, are decays by electron capture and by positron emission, in which cases argon (^{40}Ar) is produced. These decays are as follows:

$$^{40}\mathrm{K} + e^- \rightarrow {}^{40}\mathrm{Ar} + \nu_e + \gamma \tag{1.7}$$

and

$$^{40}\mathrm{K} \rightarrow {}^{40}\mathrm{Ar} + e^+ + \nu_e \tag{1.8}$$

Where e^+ is a positron, ν_e is an electron neutrino and γ is photonic radiation. In the case of electron capture (equation 1.7) only a few photons are created (if not just one), so this reaction has a fairly low chance of leading to a detection. In the case of positron emission (equation 1.8) however, the emitted positron will emit Cherenkov radiation if it has a sufficient velocity and can thereby create a signal. The chance of positron emission happening is, however, very small (a branching ratio of only 0.001%), so this decay also attributes to only a very small portion of the detections.

The second source of background radiation does, in contrast to the ^{40}K decay, fluctuate a lot in both time and space. The bioluminescence is produced when a sea current sweeps in bioluminescent organisms and they impact on the DOMs [1]. Usually the bioluminescent background comes in short but very intense bursts. To filter out these bursts a PMT will go into high rate veto when the photon rate goes over 20 kHz, which means that data acquisition will cease for that PMT for a short time. Bioluminescence is an issue for ORCA. Due to the depth, however, it has almost no effect on ARCA, since the organisms that create this light do not tend to sink this deep.

The third, and last, large source of background radiation for KM3NeT is the radiation created by atmospheric muons. As is the case for the muons created in neutrino interactions in the seawater, these atmospheric muons travel with nearly the speed

of light. Once in the water, these muons will therefore also emit Cherenkov radiation until their velocity is below the speed of light in seawater.

While these muons are considered a background source for the eventual KM3NeT experiment, they are the main signal source for this research and are useful for calibrating the DOMs [12].

Muons with sufficient energy can easily reach the detectors far below sea level. As a consequence KM3NeT only uses the data of up-going muons, as only neutrinos are able to travel through the earth without interacting and are therefore the only possible origin of up-going muons. As a result ARCA covers the southern sky and therefore complements IceCube, which covers the northern sky.

1.4 Detection

As mentioned in section 1.1 the building blocks of KM3NeT are composed of many DUs containing 18 DOMs suspended between two vertical ropes. A DOM is a glass sphere housing the 31 photomultipliers divided over 5 rings of 6 PMTs and a single PMT pointing vertically down [1]. Between the PMTs and the glass sphere is a layer of gel, to minimize scattering off the surfaces. At the top of the sphere lies the central logic board and the cable connection for both power input and data output. All these elements are shown in figure 1.2.

Although neutrinos are the signal source for KM3NeT, this setup is not built to detect neutrinos directly. This is because that can not be done due to the fact that they do not carry charge, and therefore do not couple to light. However, they can be detected when they interact with particles in the seawater. The setup is therefore designed to detect the Cherenkov radiation emitted by the resulting particles of these interactions.

1.4.1 Cherenkov radiation

When a negatively charged particle (like a muon) moves through a dielectric medium, it slightly attracts the positively charged atomic nuclei in its vicinity (a positively charged particle, such as an anti-muon, would attract the electrons, thereby causing the same effect). Due to this attraction the atom elongates and starts acting as a dipole. As such, each passing neighborhood of the muon will receive a short electromagnetic pulse. At low velocity this process is symmetric in both azimuth and along the axis of propagation. Due to this symmetry the resultant field at large distances will be equal to zero and therefore there will be no radiation [13].

The case changes when the muon travels at a high velocity, with high velocity meaning a velocity of about the speed of light in the medium. At such velocities the symmetry along the axis of propagation is lost in each individual moment due to a resultant dipole field still measurable at large distances from the muon. In this case radiation is emitted during the electromagnetic pulse, but generally the radiation from along the track of the muon interferes destructively. This means

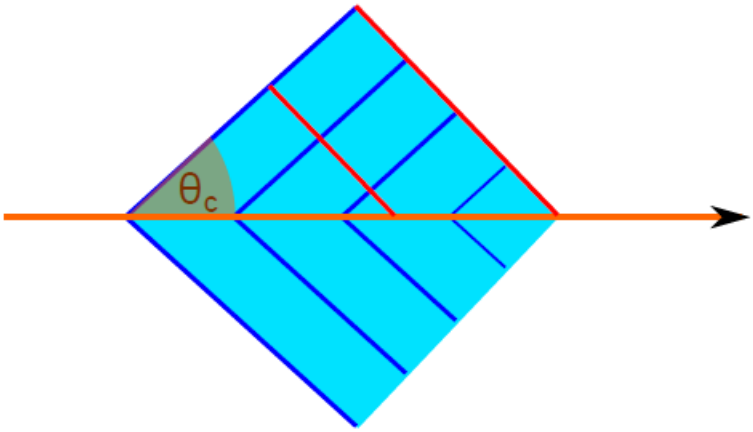

Figure 1.5: A sketch of a charged particle travelling at relativistic speed (in orange), radiated photons under Cherenkov angle θ_C (dark blue) and the surface all photons pass at the same time (red) [11].

that the resultant field intensity at a large distance is still zero. If the muon has a velocity higher than the phase velocity of light in the medium, however, there is a possibility for the radiation to interfere constructively and this radiation is known as Cherenkov radiation [13]. This situation is sketched in figure 1.5, where the charged particle (e.g. a muon) in orange emits radiation at an angle θ_C called the Cherenkov angle. This angle offset θ_C from the axis of propagation in which the Cherenkov radiation can be detected depends on the refractive index n of the medium and the velocityfactor β of the muon (where $\beta = v_\mu/c$) as following:

$$\cos\theta_C = \frac{1}{\beta n} \tag{1.9}$$

Using that the refractive index is the ratio between the speed of light in vacuum and the phase velocity ($n = c/v_p$), one can rewrite equation 1.9 to:

$$\cos\theta_C = \frac{v_p}{v_\mu} \tag{1.10}$$

In equation 1.10 one can then see that there will only be a Cherenkov angle and therefore radiation if the velocity of the muon exceeds the phase velocity of light in the medium, since $arccos\frac{v_p}{v_\mu}$ will only have a real solution if $\frac{v_p}{v_\mu} \leq 1$ [13].

1.4.2 Hit processing

As said, KM3NeT is designed to detect this Cherenkov radiation, the radiated photons are therefore responsible for (a part of) the registered detections.

Once a photon hits the photocathode (or the housing hereof) of a PMT, a cascade of electrons is generated. When the preset threshold (of typically 0.3 photoelectrons) is breached, it passes the so called zero-level (L0) filter and is registered as an L0 hit. All L0 hits are attributed three pieces of information by the central logic board: the time at which the threshold was breached, the amount of time the signal is above the threshold and the PMT address.

KM3NeT works with the "all-data-to-shore" concept, so the data of all L0 hits is sent to an onshore location for them to be processed there. The first and most important filter applied onshore is called the level-one (L1) filter. This filter looks if two or more PMTs on the same DOM had an L0 hit within a timewindow of 10 nanoseconds and if that is the case, the total is registered as an L1 hit. Only these L1 hits are then saved in timeframes of 100 ms. Consequently, the L1 filter largely suppresses the uncorrelated background, as uncorrelated L0 hits are less likely to form an L1 hit.

Since only the L1 hits are saved, all further filters to identify hits related to passing particles make use of these L1 hits.

1.5 Aim of this research

The goal of this research is to find whether one can (accurately) measure the time difference between DUs using the atmospheric muon signal. If this is possible, it would mean that in the future the atmospheric muon signal can be used for in situ (re)calibration of the detector. The expected time difference (between both different DOMs and DUs) of the muon signal are known and could therefore be used to (re)set the time on the internal clocks of the DOMs. Thereby serving as a cross-check for the onshore calibration and maybe lengthening the lifetime of the detector by keeping the clocks synchronized.

However, for such precise calibrations it is necessary to have a very clean signal. The second goal of this research is therefore to find out the effect of filtering out the data of DOMs with a loss of synchronization. And, consequentially, whether it is an important step in cleaning the muon signal alongside filtering out other background radiation.

The structure of this thesis is as follows. In chapter 1 KM3NeT was introduced by elaborating on its structure, its research goals, its signal and the processing thereof. Chapter 2 will elaborate on atmospheric muons, which are the main signal source for this research, and a muon depth dependence measurement performed by KM3NeT is discussed.

The content of the research hereafter is threefold. In chapter 3 the data selection and the occurrence of losses of synchronization will be discussed. Chapter 4 will encompass a measurement of the atmospheric muon depth dependence and the effect

hereon of such losses of synchronization. In chapter 5 the average time difference between DUs is discussed and compared to simulated data. Each chapter contains the methods, results and conclusion for that part of the research.

Chapter 2

Atmospheric muons

As mentioned in the introduction this research does not in fact solely use the data of neutrino detections, since neutrinos are simply not detected often enough to have sufficient data. Particles that are detected abundantly, however, are muons. As one can see in equations 1.1, 1.2 and 1.3, muons are often a product in the air showers created by cosmic rays interacting high up in the atmosphere. Muons are therefore produced in large quantities in our atmosphere over a wide range of energies. Due to their relativistic speed muons can easily reach the ground despite their short lifetime.

One can see in figure 2.1 that up until about 1 TeV (10^3 GeV) the path length of muons has a steep increase with increasing energy. However, from as low as the so called muon critical energy (at 500 GeV), the dominant energy loss factor is the radiative losses. These losses (such as Brehmsstralung, pair production and photonuclear interactions) have a steep increase with increasing energy and thereby slow down the increase of the path length of muons [14].

With a sufficiently high energy (of about 500 GeV or more) a muon can, however, already travel through the two to three kilometers of water above the ARCA and ORCA detectors, as can also be seen in figure 2.1.

2.1 KM3NeT muon depth dependece

In figures 2.2 and 2.3 some results of the first muon depth dependence measurement by the KM3NeT collaboration are shown. From them, the magnitude of the discussed muon abundance can also be deduced.

In figure 2.2 the average rates of L1 hits are shown as a function of the multiplicity[1] of the L1 hits in question. These rates are shown for ORCA with one active DU (ORCA1) and ARCA with two active DUs (ARCA2). The L1 hit rate is dominated by background such as ^{40}K decay up until a multiplicity of six, and by atmospheric muons above a multiplicity of seven [16]. This means that in ARCA, on average, an L1 hit with a multiplicity of 8 is created every 50 seconds.

[1]The multiplicity indicates the number of L0 hits in an L1 hit.

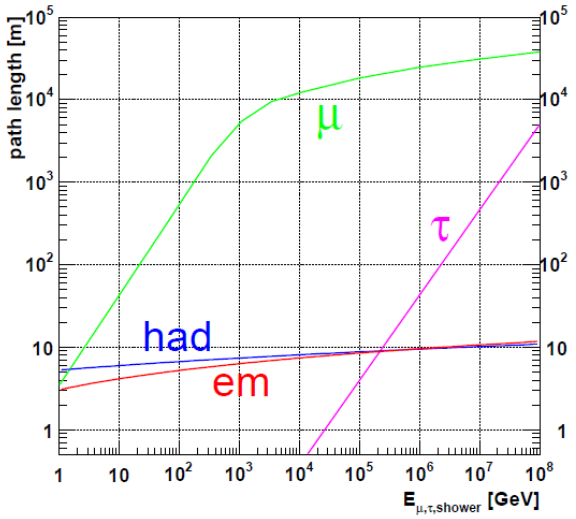

Figure 2.1: The path length of taus, muons and hadronic and electromagnetic showers created in neutrino interactions in the seawater as a function of their energies [15].

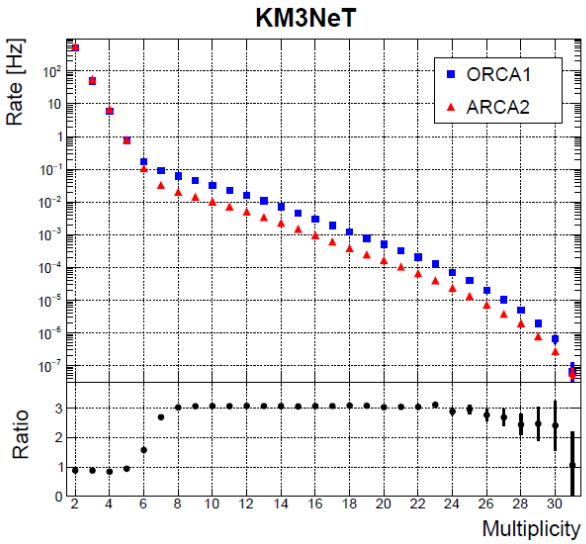

Figure 2.2: Top: The average L1 hit rates as a function of the multiplicity for both ORCA1 and ARCA2.
Bottom: The ratio between the L1 hit rates of both detectors [16].

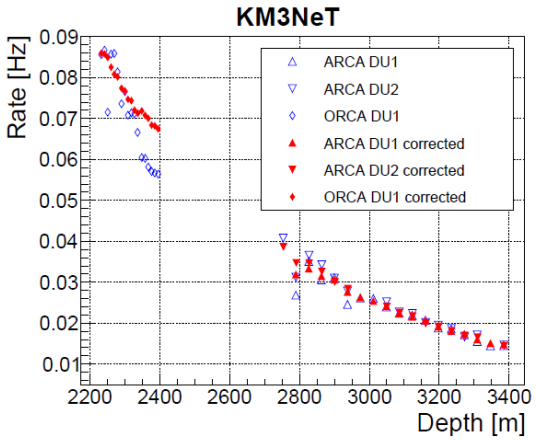

Figure 2.3: The average L1 hit rates for all DOMs in ORCA1 and ARCA2 with a multiplicity ≥ 8 as a function of their depth [16].

In figure 2.3 one can see that the muon rate decreases (exponentially) with depth and halves roughly every 450 meters (e.g. roughly 0.08 Hz at 2300 m, roughly 0.04 Hz at 2750 m and roughly 0.02 Hz at 3200 m). One can also see that where the corrected rates vary little from the uncorrected rates at larger depth in ARCA, the upper DOMs of ARCA (at depths of about 2750 - 2950 m) deviate more. The correction shown here is based on the efficiencies of the PMTs in the DOM. Since a lower rate will be measured with a lower average PMT efficiency of the DOM (and a higher rate with a higher average PMT efficiency), the rates are corrected to how they would be if all efficiencies were identical.

The absence of data points between the depths of 2400 to 2700 m can be explained

by the absence of DOMs at these depths. The seafloor at the ARCA site is about one kilometer deeper than at the ORCA site and ARCA is only about 700 m high.

2.2 Incidence angles

Since cosmic rays can interact in any place in the atmosphere and their products can go in all directions, the muons detected in ARCA originate from all directions. The most common trajectory of muons reaching the detector is, however, a vertical one. The trajectory of the muon defines the time difference between the detections of the photons radiated by the muon. Therefore, the measured time differences between DOMs can be used to accurately calculate the point of origin of the muon.

Given that the muon travels faster than the phase velocity of light, it can be derived that the largest time difference occurs when the photons travel parallel to the DU. In this case, given that the refractive index of seawater is about 1.34,
$|\Delta t| = \frac{|\Delta d|}{v_p} = \frac{|\Delta d|}{c/n} = \frac{36\text{m}}{c/1.34} \approx 160$ ns, this is also illustrated in figure 2.4a.

In the case the muon travels straight down (which is, as mentioned, the most occurring case) the measured time difference is slightly smaller, as can be seen in figure 2.4b. Since the muon is now travelling parallel to the DU, the measured time difference is also defined by its velocity: $|\Delta t| = \frac{|\Delta d|}{c} = \frac{36\text{m}}{c} \approx 120$ ns.

When the muon comes in at exactly the Cherenkov angle, so that the photons travel perpendicular to the DU, the time difference is 0 ns. If the incidence angle exceeds the Cherenkov angle the time difference can even become positive, since the photons radiated by this muon can have an upward trajectory. These cases are illustrated in 2.4c and 2.4d, respectively.

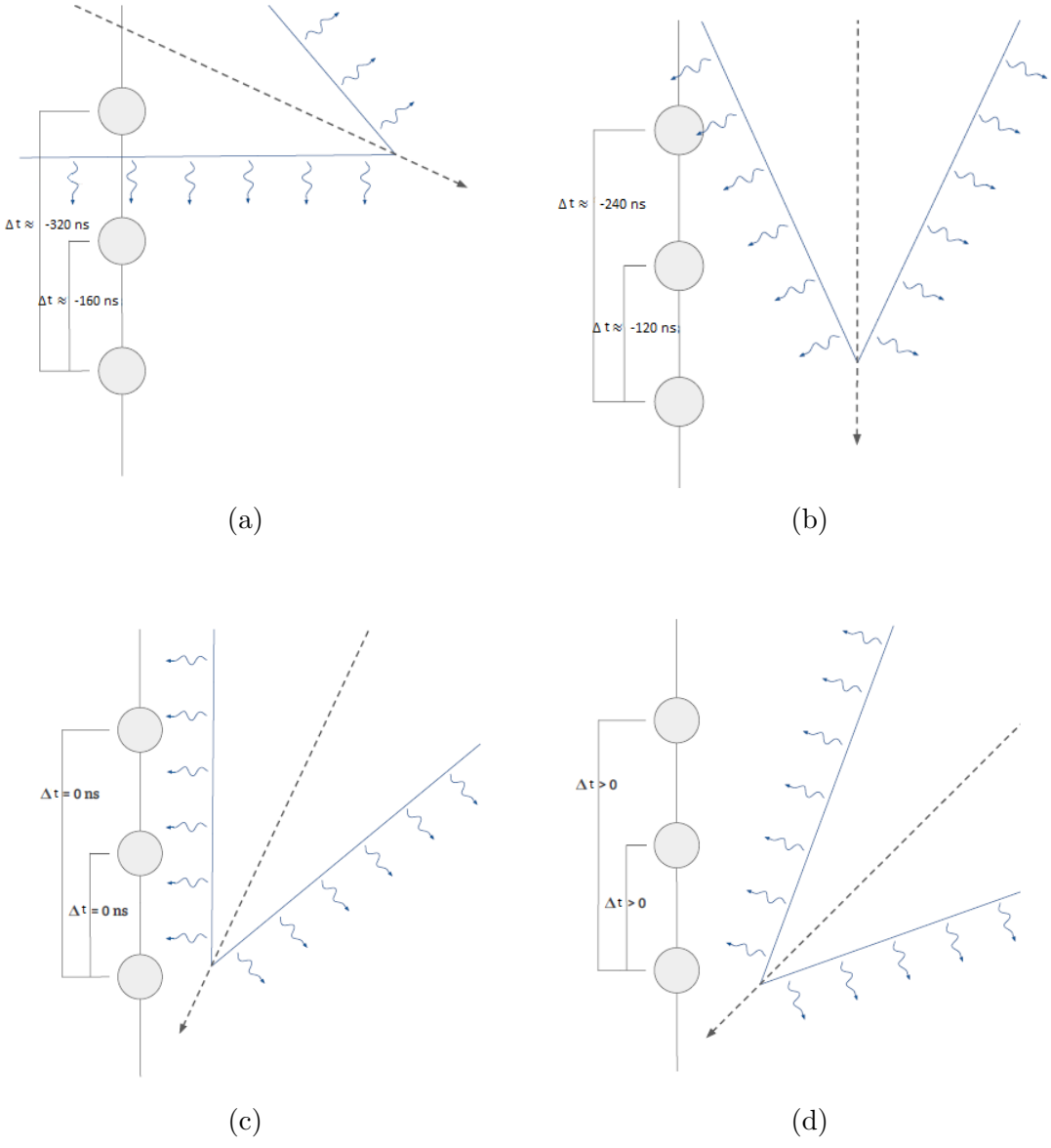

Figure 2.4: Different incidence angles of muons, causing distinct time differences between the DOMs. The largest negative Δt caused by vertical photons in (a), the most common case (that of vertical muons) in (b), $\Delta t = 0$ ns by horizontal photons in (c) and $\Delta t > 0$ ns by photons with upward trajectories in (d) [12].

Chapter 3

Data sample and selection

In this research the data from December 23, 2016 to February 3, 2017 of the ARCA detector was evaluated. During this time period ARCA had two working DUs in the sea (DU1 and DU2).

In the KM3NeT detector, a malfunction sometimes occurs in which the internal clock of a DOM temporarily loses synchronization with the rest of the detector will be evaluated in this chapter. When such a malfunction happens, the L0 (and therefore the L1) hits the DOM detects are given a wrong timestamp. This wrong timestamp has as an effect that all time comparisons with L1 hits of this DOM are nonsensical, since these L1 hits are in fact detected at a different time. The procedure to counter the influence of these synchronization losses will be discussed in this chapter.

3.1 Methods

3.1.1 Data

To determine how big the effect of DOMs with a loss of synchronization is, 169 runs worth of ARCA data are evaluated. A run is a period of data-taking and there are two types of runs: physics runs and calibration runs. The physics runs (usually) have a duration of a few hours and during them only the L1 hits are saved, as

	period	runs	total runtime	number of functional runs	functional runtime
phase 1-3	23-12-2016 - 14-01-2017	5009 - 5100	20.12 days	83	19.62 days
phase 4	14-01-2017 - 03-02-2017	5103 - 5233	18.16 days	86	17.66 days

Table 3.1: General information of used phases.

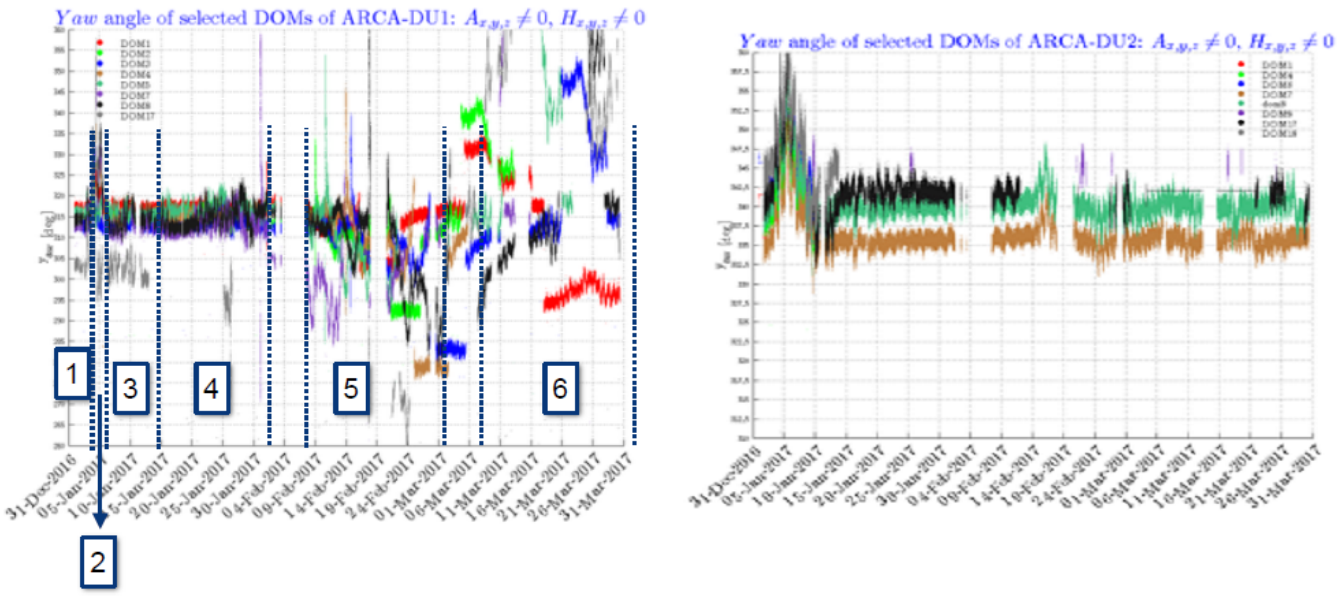

(a) (b)

Figure 3.1: The yaw angle of a selection of DOMs as a function of time. In (a) DOMs of DU1 are shown and the phase division is illustrated. In (b) DOMs of DU2 are shown [17].

discussed in section 1.4.2. The calibration runs are a lot shorter (only a couple of minutes) and during these runs all L0 hits are saved, since these are useful for the calibration of PMTs. These calibration runs are not used in this research.

The 169 runs are divided over 4 so called phases. These phases are collections of runs divided as such based on the movements of the DUs by R. Coniglione [17], this division can be seen in figure 3.1a. Since the rate calculation is done under the assumption of a stable position of the DOMs, one would want to work with datasets that have as little movement within them as possible. Compared to the yaw angles[1] shown in figure 3.1, which change quite a lot between the first three phases, the roll and pitch angles[1] are fairly stable over the time span of the four evaluated phases.

Having two DUs means there are 36 DOMs connected to their lines. For simplicity the numbering of these DOMs is continued over the DUs, this means that DOM 19 is the lowest DOM on DU2. However, some of these DOMs of DU1 and DU2 broke before or during the runs evaluated in this research, the DOM in question is then listed as "dead". DOMs 18, 20, 29 and 30 were "dead" since before this data was taken. Connection was lost with DOM 34 during phase 1 and in between phase 3 and 4, the connection with DOM 19 was also lost.

Incidentally a DOM malfunctions so that communication is temporarily lost. This differs from a loss of synchronization as with this malfunction no data is acquired during the run at all. This malfunction happened to DOM 7 in runs 5098 and 5099 and to DOM 24 in run 5129. A visual representation of all dead DOMs and unused runs can be seen in figure 3.2.

In figure 3.3 the runtimes of all the runs are depicted. Since the rate of L1 hits is fairly stable over time, the runtime is the main limitation on the number of L1 hits detected in the run.

[1]The roll, pitch and yaw rotations are rotations around the x, y and z axes, respectively.

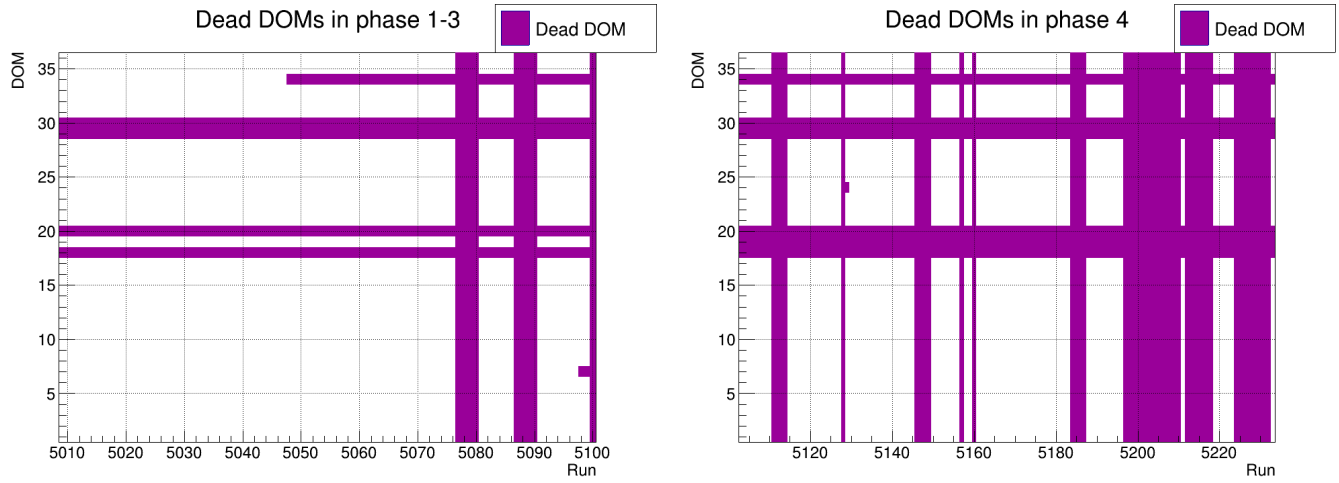

(a) (b)

Figure 3.2: Dead DOMs as a function of the run number. For simplicity the calibration runs are also defined as fully dead (which account for the vertical bars).

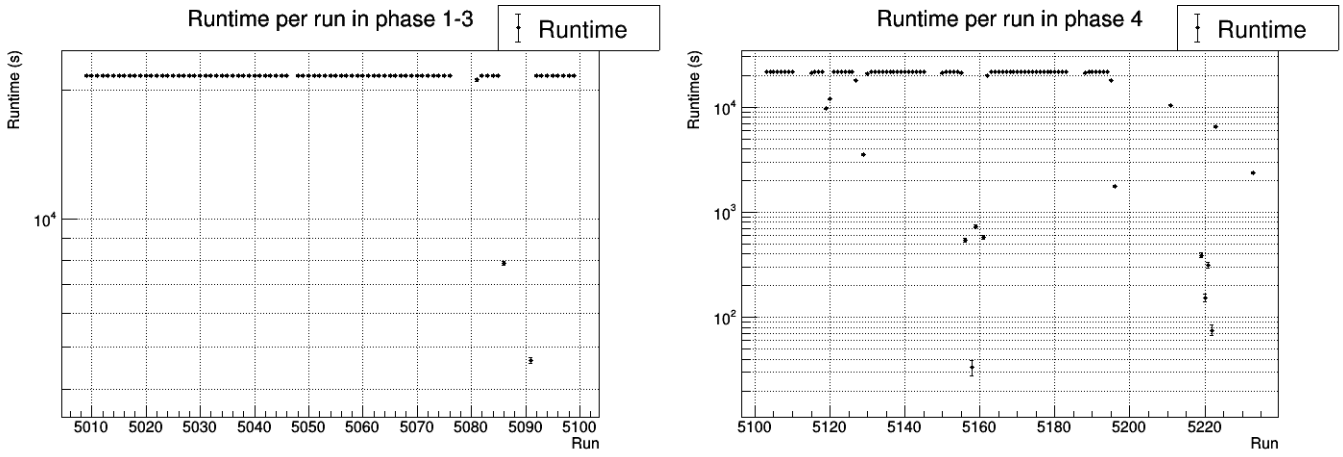

(a) (b)

Figure 3.3: The runtimes as a function of the run number. The statistical errors are included but (mostly) smaller than the markers.

3.1.2 Inventory of DOMs with a loss of synchronization

Whether a DOM has a temporary loss of synchronization or not is determined using the existing software JTurbot, developed by M. de Jong. In JTurbot, the time differences are calculated between so called triggered hits and L1 hits on the DOM. In which a triggered hit means a (group of) L1 hit(s) that passed another filter, this triggered hit will also be given its own mean hit time. In the case of a triggered hit all DOMs in both the DUs are expected to have an increase in L1 hits, so a peak will be registered at the mean hit time of the registered hit.

If a DOM has a loss of synchronization, however, the L1 hits will have been given a wrong timestamp and the peak in L1 hits will therefore not be at the mean hit time of the registered hit. A DOM is therefore deemed to have a loss of synchronization when its peak in L1 hits is too far removed from the mean hit time of the registered

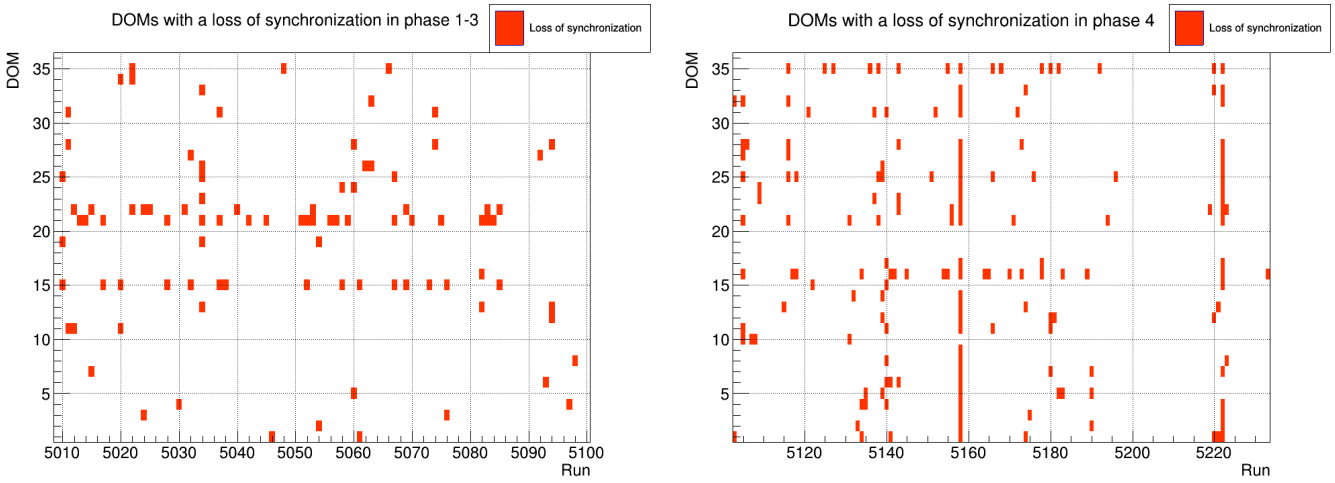

(a) (b)

Figure 3.4: DOMs with a loss of synchronization as a function of the run number.

hit. In JTurbot "too far" is defined as more than 50 ms away. In figure 3.4 a visual representation is given of which DOMs were deemed to have such a loss of synchronization by JTurbot.

3.1.3 Coincidences

The evaluation of the stored L1 hits in a run was executed using the existing software MonitorL1dt, developed by K. Melis. This routine provides two-dimensional histograms, in which the time differences between the L1 hits on different DOM pairs are filled. Such a combination of two L1 hits on two different DOMs is called a coincidence from here forward. Therefore, these histograms show the time differences in the coincidences with a DOM.

In figure 3.5a such a histogram is shown (in this case the coincidence histogram of DOM 1 in run 5034). This means that in this histogram the time differences are shown of the coincidences with DOM 1.

In it, no entries are seen in the first column between $\Delta t = -1000$ and $\Delta t = 1000$ ns. This is due to the fact that MonitorL1dt only registers the first L1 hit every 1000 ns, which is to make sure that one muon will only account for one L1 hit per DOM. This inherently means that within 1000 ns on the DOM for which the coincidences are calculated there can be no coincidences, since there are no other registered L1 hits in this timewindow. No entries are seen either in columns 18, 20, 29 and 30, which is because these columns represent the dead DOMs and will therefore not create any coincidences.

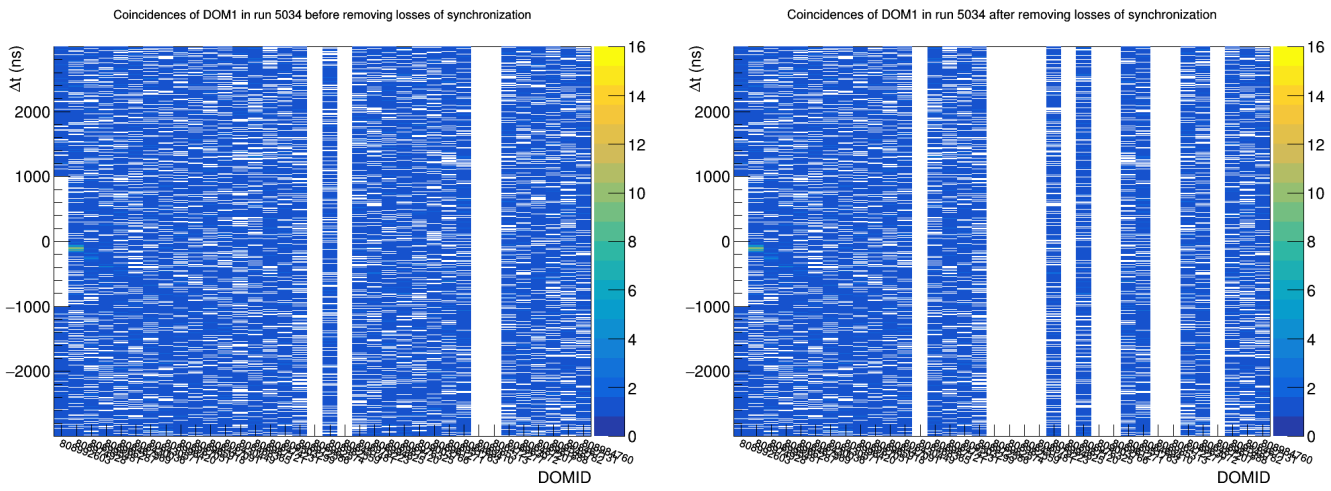

(a) (b)

Figure 3.5: The number of coincidences of DOM 1 in run 5034 as a function of the hit time difference and the DOM the coincidence is with, both before (a) and after (b) removing the coincidences with DOMs that had a loss of synchronization.

3.2 Results

The easiest way to see the direct effect of a DOM that has a loss of synchronization is to compare the coincidence histograms of a DOM before and after removing the data of DOMs with a loss of synchronization. In figure 3.5a the coincidence histogram is shown for DOM 1 in run 5034 as explained in section 3.1.3. In figure 3.5b the coincidences of the same DOM in the same run are shown, but after removing the coincidences with the DOMs that had a loss of synchronization. One can see 7 more DOMs without coincidences in 3.5b than in 3.5a, since there are 7 DOMs with a loss of synchronization in run 5034 (as one can see in figure 3.4).

In figure 3.6 the total amount of coincidences and the amount of removed coincidences due to DOMs that had a loss of synchronization are shown for each run. Needless to say, if not a single DOM had a loss of synchronization in a run, no coincidences are removed. In this case the amount of removed coincidences is not plotted.

In figure 3.7 this combination of total and removed coincidences is translated into the percentage of coincidences that are removed. The percentages seem to increase discretely, this is caused by the fact that the coincidence count is dominated by background radiation due to the low minimal multiplicity. Since the background is roughly constant over time and space, every loss of synchronization has roughly the same impact on the removal percentage, regardless of the muon flux.

The extremely high percentages in runs 5158 and 5222 can be explained by the combination of their short runtime and high amount of DOMs that had a loss of synchronization (as can be seen in figures 3.3b and 3.4b, respectively).

The removed coincidences account for a total of 6.2% and 8.1% of all coincidences in phase 1-3 and phase 4, respectively.

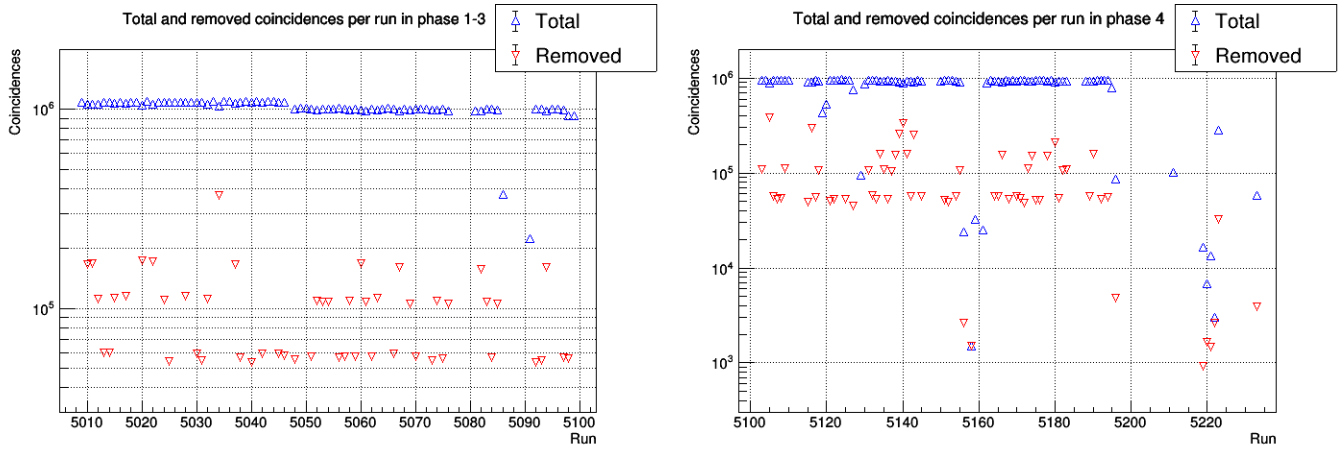

(a) (b)

Figure 3.6: The total number of coincidences and the number of coincidences that are removed due to the loss of synchronization of a DOM, both as a function of run number. Only nonzero removal counts are shown. The statistical errors are included but smaller than the markers.

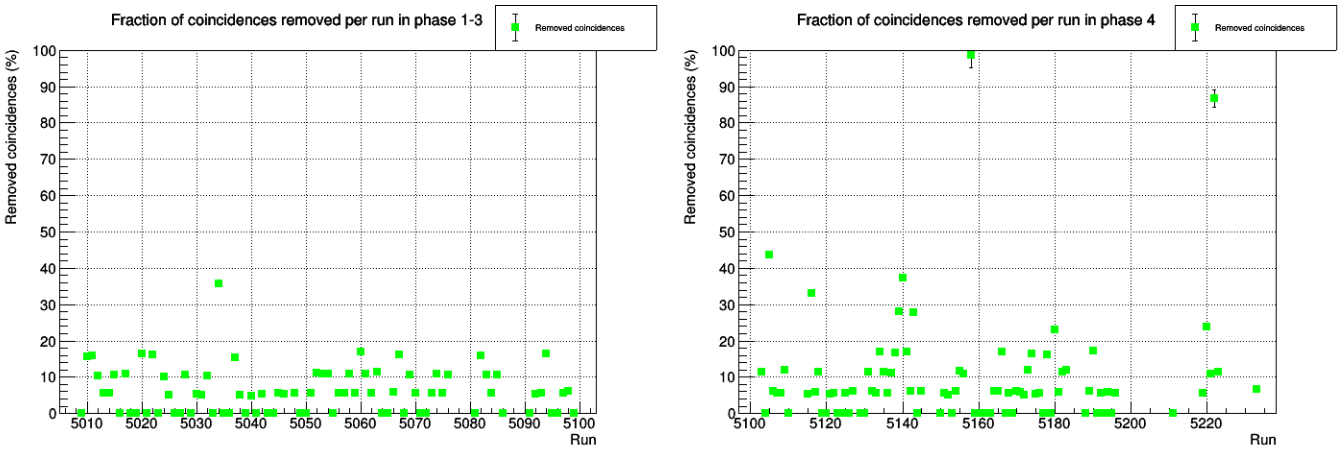

(a) (b)

Figure 3.7: Percentage of the total of coincidences that was removed because of a loss of synchronization as a function of the run number. The statistical errors are included but (mostly) smaller than the markers.

3.3 Conclusion

The losses of synchronization have a significant impact on the data, due to large amount of coincidences that have no physical value because of the wrong timestamp they are given. Since the background is the dominant source of coincidences here, it might however be interesting for future research to asses the impact at a higher multiplicity, in which case the background is further suppressed.

The effect these losses of synchronization have on the muon depth dependence will be discussed in the next chapter. Whereas all coincidences were included in this determination of the impact of losses of synchronization, only the correlated signal

will be included in the next chapter. Therefore, this will give an extra measure on the impact DOMs with a loss of synchronization have on the muon signal.

Because of the frequent occurrence of losses of synchronization and their significant impact on the data, the data after the removal of losses of synchronization is significantly cleaner than before this removal. Therefore, the results presented here already give enough reason to use the data after this removal in chapter 5.

Chapter 4

Atmospheric muon depth dependence

In this chapter a method will be described to measure the depth dependence of atmospheric muons by making use of the time correlations between the L1 hits in different DOMs as a measure of the amount of muons at a given depth. The effect of losses of synchronization on this measurement will then be discussed. At the end of the chapter, the results will also be compared to the muon depth dependence performed by the KM3NeT collaboration.

4.1 Methods

4.1.1 Data

For measuring the atmospheric muon depth dependence all the same runs were evaluated as were in chapter 3, so the general info can be found in table 3.1. For this part all the runs of phases 1-3 are added together into one file (as are all the runs of phase 4) for better statistics. The depth dependencies are calculated both with and without the exclusion of DOMs with a loss of synchronization, to serve as a test of the effect these losses of synchronization have on the muon signal.

4.1.2 Correlation

The muon rate at a certain depth can be measured through the amount of correlated L1 hits the muons create at that depth. Therefore, the correlation rate of DOM i with DOM j (where DOM j is the upper vertical neighbor of DOM i) will be used as a measure of the the muon rate at the height of DOM i.

The coincidences are once again calculated using the software MonitorL1dt by K. Melis. Since the interest now lies in the correlations of a DOM with its upper neighbor to measure the muon rate at that height, a projection is taken of the two-dimensional histogram (which can be seen in figure 4.1) of the column representing

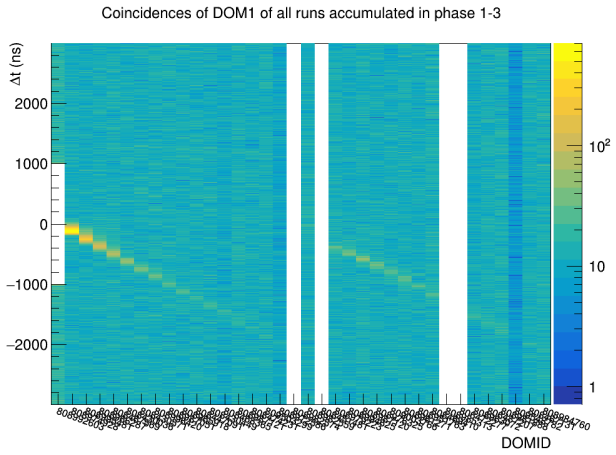

Figure 4.1: The number of coincidences of DOM 1 in phase 1-3 as a function of the hit time difference and the DOM the coincidence is with.

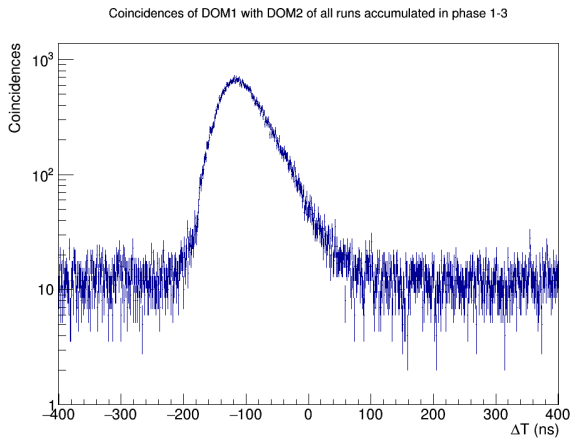

Figure 4.2: The distribution of the time differences of L1 hits in DOM 1 and DOM 2.

the neighboring DOM. This gives us a histogram as in figure 4.2, which in this case shows the correlations of DOM 1 with DOM 2 in phase 1-3. Both figures 4.1 and 4.2 display the coincidences before the removal of data from DOMs with a loss of synchronization.

The correlation rate is then calculated by first integrating the projected coincidence histogram over a window of 500 ns around the top of the peak seen in figure 4.2. This window is placed from 200 ns before to 300 ns after the top of the peak. The window is chosen as such because the maximum photon arrival time difference between neighboring DOMs is measured when the photons travel vertically, in which case $|\Delta t| \approx 160$ ns. The larger margin on the positive side of the peak is to include the observed elongated tail, of which the coincidences are still correlated signal from the passing muons.

Secondly, the average background for 500 ns is subtracted, to assure the background will not attribute to the muon rate. This average background is calculated by integrating the projected coincidence histogram over a window of 500 ns at a large time offset ($\Delta t = 1000$ - 1500 ns).

Finally, the correlation count is divided by the total runtime of that DOM in the phase in question to get the average correlation rate. For the calculation of the correlation rate before the removal of losses of synchronization, this total runtime is the accumulation of the runtimes of all the evaluated runs in the phase. For the calculation after this removal, the total runtime is the accumulation of the runtimes of all runs in which the DOM did not have a loss of synchronization.

4.1.3 Depth dependence

The atmospheric muon rate is expected to decrease with depth due to the higher energy required to reach that depth. This decrease will approximately be an exponential decay, as can also be seen in the results of the muon depth dependence by

KM3NeT (in figure 2.3). For this reason a simple exponential is fitted to the signal:

$$rate \;=\; e^{a \,+\, bx} \tag{4.1}$$

Wherein e^a is the scaling factor, b determines the slope of the exponential and x is the height above the seafloor. The length it then takes for the signal to halve is described as:

$$H_{1/2} \;=\; \frac{ln(2)}{b} \tag{4.2}$$

Nota Bene: the rates calculated in this research are not the actual muon flux, but the rates of correlations created by these muons. Therefore, this distance $H_{1/2}$ is not the actual decay length of the muons, but the length over which the correlation rate caused by these muons halves.

4.2 Results

The measured muon depth dependencies are shown in figure 4.3. As one can see, the muon rates are corrected to a higher value after the removal of DOMs with a loss of synchronization from the data and the χ^2 value of the fitted exponential is consistently lower after this removal. Besides that, the slope (and therefore the halving distance) is also more stable after the removal of losses of synchronization.

The measured halving distance is slightly lower in phase 1-3 than in phase 4, and slightly lower in DU2 than in DU1. It is visible, however, that the muon rates measured in the DOMs toward the top of both DUs deviate from the fitted exponential considerably, and that these deviations persist after the removal of DOMs with a loss of synchronization.

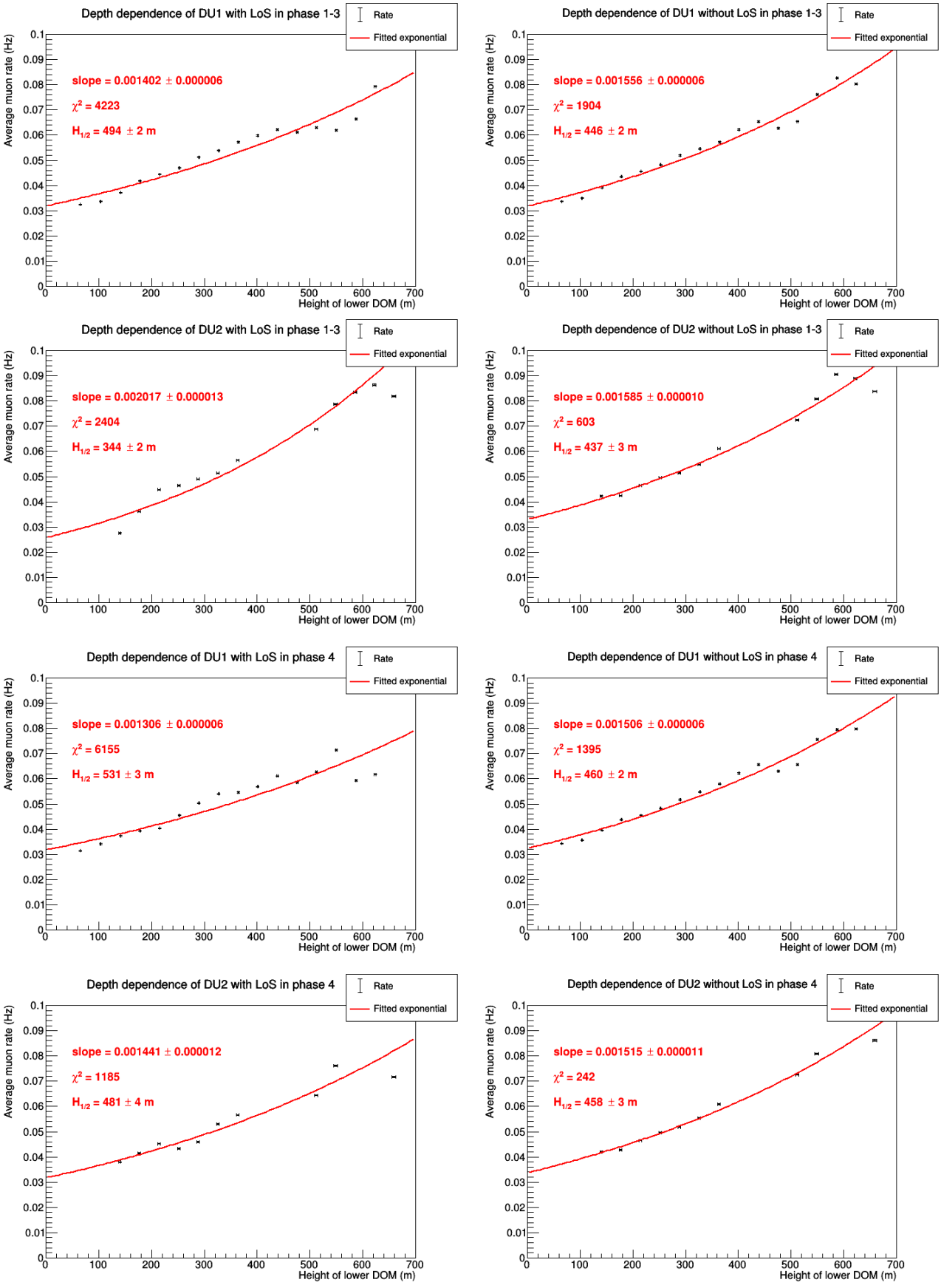

Figure 4.3: The average muon rate as a function of the height off the seafloor for both DUs in both phases, both before (left) and after (right) the removal of DOMs with a loss of synchronization. A simple exponential is fitted to the data (in red).

4.3 Conclusion

The higher muon rates after the removal of the losses of synchronization are as expected, since no correlated signal is produced in a DOM that has a loss of synchronization. This absence of correlated signal lowers the muon rate when the runtime of the run in which the DOM has a loss of synchronization is included in the calculation of this muon rate. The consistently lower χ^2 values after the removal of DOMs with a loss of synchronization also indicate that the exponential fit is a better representation of the data after this removal than before it. The more stable values for the slope and halving distance after the removal indicate that the four different calculations are more in agreement than the four calculations before removing the data of DOMs with a loss of synchronization. These three changes together mean that the data without the DOMs that had a loss of synchronization gives a more true to nature muon depth dependence.

However, even after the removal of DOMs with a loss of synchronization, the exponential fit does not match within the statistical error margins at all heights. This could be explained by differing efficiencies of the PMTs. In this research all PMT efficiencies were assumed to be identical, which they are not. A slightly higher efficiency of the PMTs in a DOM would cause a slightly higher correlation rate with that DOM, so a difference in the average efficiency of DOMs would cause deviations from the average muon depth dependence.

These deviations from the exponential fit are significantly larger at the higher DOMs, which means the difference in the average PMT efficiency of these upper DOMs are larger. This can also be seen in figure 2.3, where one can see that the rates of the upper DOMs of ARCA are corrected significantly more than the DOMs at larger depths.

The difference in halving distances between the DUs could also be explained by a difference in PMT efficiencies, as higher average efficiencies in the upper DOMs of DU2 would cause the measured halving distance to decrease (as lower efficiencies in the top of DU1 would increase the measured halving distance). Since the corrections to the rates (as seen in figure 2.3) are significant, these corrections would also significantly influence the slope of the exponential. The error on the halving distance caused by differing PMT efficiencies is therefore of the order of several meters.

The difference could also be explained by more movement in DU1, since a horizontal movement of a DU would also slightly decrease the height of the DOMs in that DU. These heights are however assumed to be unchanging. At the slightly larger depth the DOM will measure a slightly lower muon rate than at the height it was assumed to be. Since this difference in height is larger for the higher DOMs, this causes the slope of the muon depth dependence to decrease a little. It would therefore cause the halving distance measured in that DU to increase with a few meters.

The difference in halving distance between the two phases, combined with the fact that phase 4 has little movement in it (as explained in section 3.1.1), could imply two possible effects. Either a stable inclination in both DUs in phase 4 larger than the inclinations in phase 1-3, or a fast decrease in PMT efficiencies in the upper DOMs of both DUs. Further research could evaluate whether and how these effects

are affecting the muon depth dependence measurement.

Comparing the measured halving distances between 437 and 460 m to the halving distance of roughly 450 m found by the KM3NeT collaboration, shows that despite of the different methods used in the measurements of the muon depth dependence, the results are rather comparable. The measurement of the KM3NeT collaboration makes use purely of the number of L1 hits with a multiplicity ≥ 8 on a DOM as a measure of the muon rate at the height of that DOM, whereas this research uses the correlation rate of a DOM with its upper neighbor with a multiplicity ≥ 2 as a measure for the muon rate. Because of these different methods, the dependence of the average DOM efficiencies on the energy and the incidence angle of a muon could also be different. Besides that, the method used in this research makes it more susceptible to the effect of DOM malfunctions and variations in PMT efficiencies. This because the calculations of muon rates at two heights are affected by a single malfunction and the average efficiency of two DOMs affect the muon rate measured at a single DOM. It however also makes this research more sensitive to muons passing the detector at a larger distance, as less radiated photons need to reach the detector.

In future research, the corrections for PMT efficiencies could be implemented in this method for a more precise muon depth dependence measurement.

Chapter 5

Inter-DU time difference

In this chapter a method is described to use the time correlations between L1 hits in different DOMs to determine the relative time offset between the two DUs. The average time differences measured in the detector data and in the simulated data are also compared to see if the simulation disagrees with the data acquired in the detector.

5.1 Methods

5.1.1 Data

For this part of the research only the data of phase 4 after the removal of losses of synchronization was used. Only phase 4 was chosen because in phase 1-3 there was still quite a lot of movement in the DUs, caused by the sea currents. This movement could affect the time difference measured between the two DUs, so these runs were rejected for this part of the research.

39 Monte Carlo runs (simulated data) were also evaluated. Since the simulation assumes perfect synchronization, the time difference between the two DUs should be zero nanoseconds in the simulation. Therefore, the simulation can be used as a measure of the accuracy of this method.

	runs	number of functional runs	functional runtime
Monte Carlo	5103 - 5195	39	5.48 days
phase 4	5103 - 5233	86	17.66 days

Table 5.1: General information of used datasets.

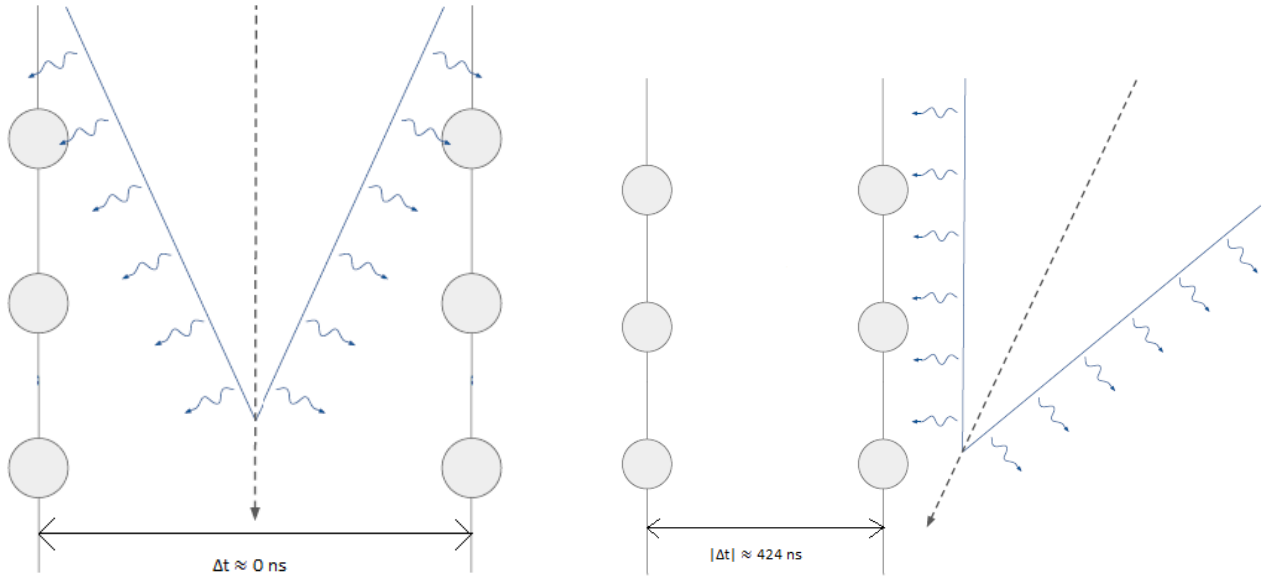

(a) (b)

Figure 5.1: The two cases causing the minimal and (approximated) maximal time difference between the two DUs: $\Delta t = 0$ ns, caused by muons passing through the line segment bisector, in (a) and $|\Delta t| \approx 424$ ns, caused by muons passing through the DU axis outside the span of the two DUs, in (b).

In the following, four different evaluations of the time correlations will be used: the coincidences with a multiplicity ≥ 2 after the removal of losses of synchronization, the coincidences with a multiplicity ≥ 4 without this removal, and the Monte Carlo data with both a multiplicity ≥ 2 and a multiplicity ≥ 4.

Effectively all coincidences with a DOM that has a loss of synchronization are background and the higher multiplicity already greatly suppresses the background. Therefore, the effect of DOMs with a loss of synchronization on the time difference calculation was expected to be minimal in the case of this higher multiplicity. Because of this it was chosen to use the coincidences with a multiplicity ≥ 4 without the removal of losses of synchronization.

5.1.2 Expected time difference signature

All locations high up in the atmosphere are assumed to have an equal chance of hosting an interaction with cosmic rays, the muon flux is therefore independent of the DU's location on the seafloor. Under this assumption of an isotropic muon flux, one would expect a Gaussian distribution around $\Delta t = 0$ in the time difference between two DOMs at the same height (on the same floor) on two different DUs. This Gaussian distribution can be exploited to try to measure the time difference between the two DUs.

The minimal time difference $\Delta t = 0$ occurs when a muon passes through the axis formed by the line segment bisector between the two DUs. In that case the travelling distances of the photons are equal from the muon to both the DUs.

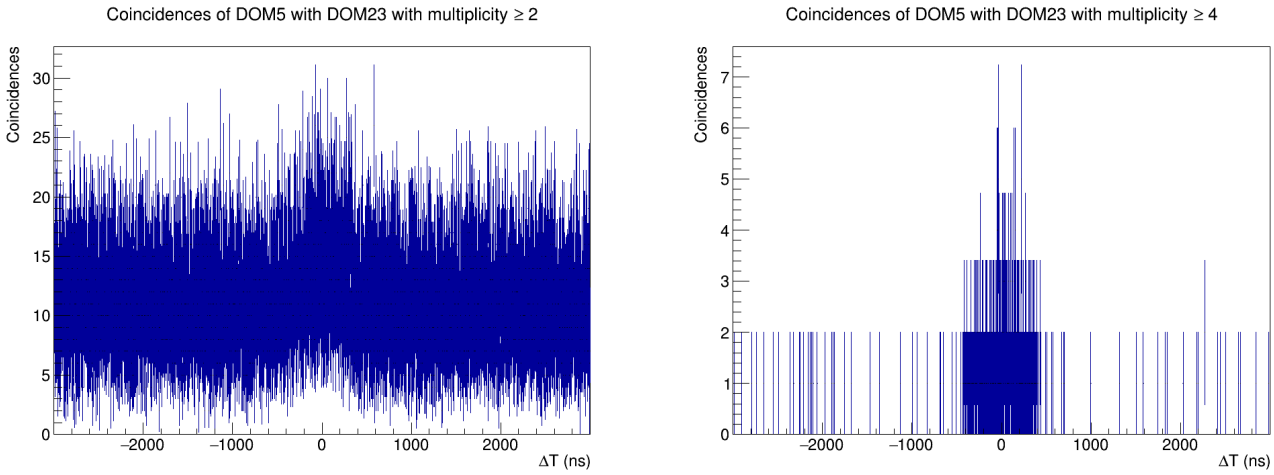

(a) (b)

Figure 5.2: The distribution of the time differences of L1 hits in DOM 5 and DOM 23. With a multiplicity ≥ 2 in (a) and a multiplicity ≥ 4 in (b).

A good approximation for the maximal time difference is the case of horizontal photons radiated by a muon passing through the axis formed by the two DUs (where both DUs lie on the same side as seen from the muon). In this case the time difference can be calculated the same way it was in section 2.2: $|\Delta t| = \frac{|\Delta d|}{v_p} = \frac{95\text{m}}{c/1.34} \approx 424$ ns. Both these cases are illustrated in figure 5.1

5.1.3 Correlation

Because the interest now lies in the coincidences between DOMs that are on the same height, the projection is taken of the column representing the DOM on the same floor, on the other DU. This is done only for the DOMs on DU1, since the absolute value of the time difference would be the same when measured from DU2 to DU1.

These histograms are then rebinned so that five bins in the original histogram form one bin in the new histogram. This is done to boost the muon signal and to make sure that the Gaussian fitted next finds the global maximum, instead of a local maximum (which happened often without rebinning). The result of this can be seen in figure 5.3. The mean of the Gaussian is then taken to be the average time difference between the two DOMs.

To have an average time difference between the two DUs as a whole, all the coincidences between two DOMs on the same floor are added together. That is to say, the coincidences of DOM 3 with DOM 21 are added to the coincidences of DOM 4 with DOM 22, et cetera. This time, however, the histogram is not rebinned, as the accumulation of the 12 functional floors already boosts the signal enough. As before, a Gaussian is fitted to the accumulated coincidences of all floors and the mean of this Gaussian is then defined the average time difference between the two DUs.

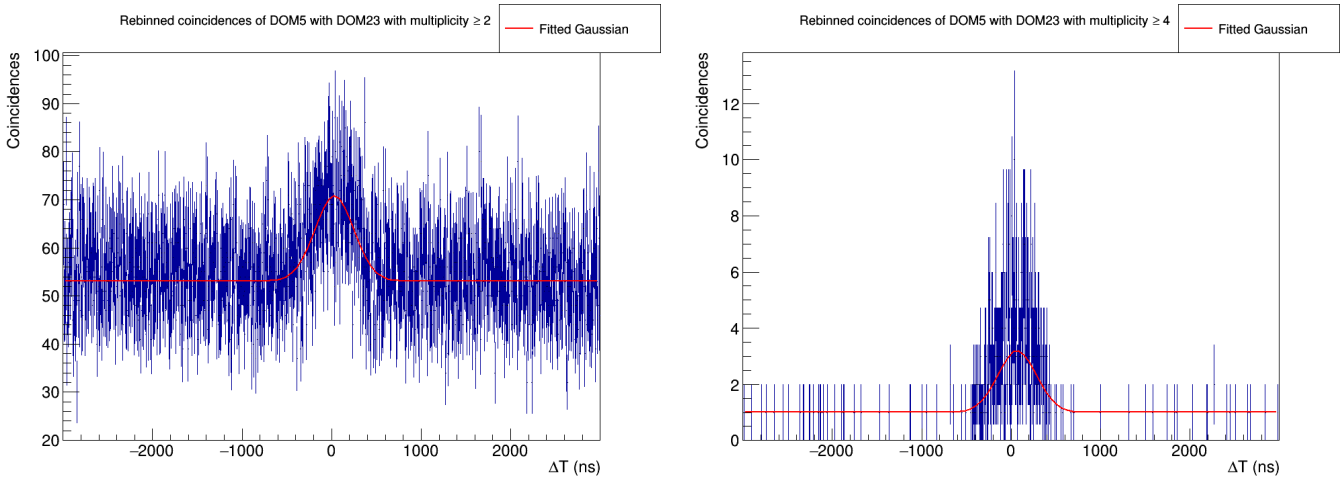

(a) (b)

Figure 5.3: The distribution of the time differences of L1 hits in DOM 5 and DOM 23 after rebinning. With a multiplicity ≥ 2 in (a) and a multiplicity ≥ 4 in (b). A Gaussian is fitted (in red).

5.2 Results

In figure 5.4 the time differences between the DUs are shown for each floor and for the DU as a whole. In the detector an average time difference between the whole DUs of 30.5 ± 0.4 ns was measured for a multiplicity ≥ 2 and a time difference of 37.4 ± 2.5 ns for a multiplicity ≥ 4. In the simulation a time difference of -11.1 ± 1.5 ns was measured for a multiplicity ≥ 2. A calculation of the time difference for a multiplicity ≥ 4 could not be made for the simulation due to the fact that the files necessary for this calculation were relocated and could not be recovered in time. However, by eye an estimation can be made that the time difference is less than 5 ns and the error is of a similar size as the error on the time difference for multiplicity ≥ 4 in the detector.

Since only the statistical errors are calculated, the size of the error depends greatly on the number of coincidences. In the detector at a multiplicity ≥ 2 this number of coincidences is high because of the uncorrelated background. In the simulation only a correlated signal is produced, the errors are therefore larger. At a multiplicity ≥ 4 the background is suppressed in the detector as well, the errors are therefore of similar size in both the detector and the simulation.

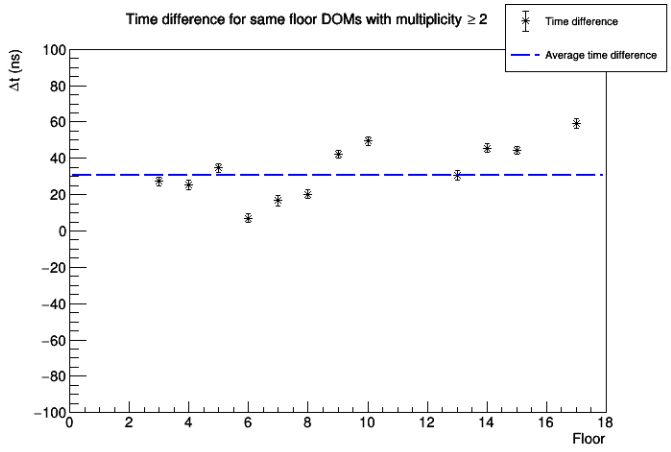

(a) multiplicity ≥ 2

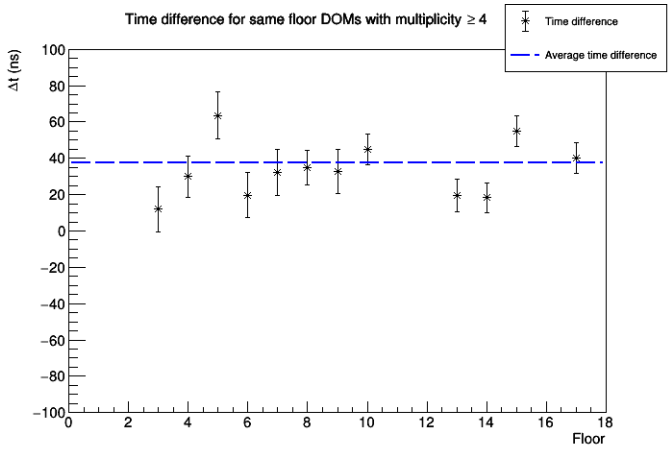

(b) multiplicity ≥ 4

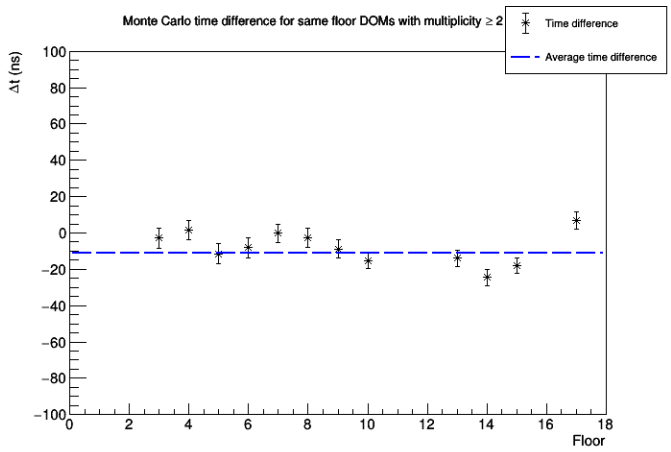

(c) Monte Carlo multiplicity ≥ 2

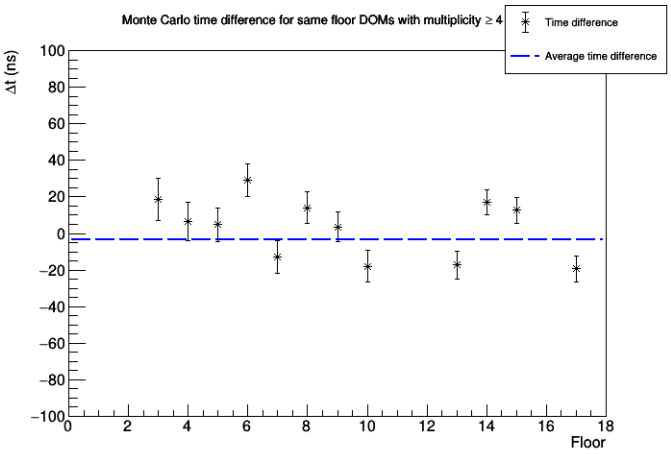

(d) Monte Carlo multiplicity ≥ 4

Figure 5.4: The time difference between two DOMs on the same floor as a function of the floor they are on. The blue dashed line illustrates the time difference in the case the data of all floors is added together.

5.3 Conclusion

The time difference measured in the simulation at a multiplicity ≥ 4 is compatible with the expected zero nanoseconds, the time difference at a multiplicity ≥ 2 is not though. Furthermore, in all four evaluations significant deviations from the DU time difference are present at single floors. These deviations could be caused by differing PMT efficiencies, then the deviations should however be comparable in the detector and the simulation, as the simulation takes the PMT efficiencies into account.

This shows that this method is not yet precise enough for the required accuracy of the time calibration. Future research could attempt to increase the precision of this method by correcting for the PMT efficiencies.

The measured time difference in the detector of about 30 ns could be caused by either a thus far undetected issue in the processing of the data (such as a wrong time calibration) or the relative movement of the DUs. The increase in distance between the DUs would have to be $|\Delta d| = v_p \times |\Delta t| = \frac{c \times 30\text{ns}}{1.34} \approx 6.7$ m to create a

time difference of this size.

Future research could make a comparison between the time differences found with this method and inter-DU distance measurements via acoustic data to verify whether DU movement is responsible for the measured time difference.

Altogether, the atmospheric muon signal is useful in various manners for scrutinizing the detector performance. Because of a muon's ability to create L1 hits in entire DUs within a few milliseconds, its signal can be used to pinpoint occurrences of losses of synchronization and to measure time offsets between DOMs at various relative orientations. Through the use of the muon depth dependence, measurements of PMT efficiencies can also be made. Therefore, the muon signal could possibly contribute to the calibration of both time offsets (between DOMs as well as DUs) and PMT efficiencies.

Bibliography

[1] S. Adrián-Martínez et al. "Letter of intent for KM3NeT 2.0". In: *Journal of Physics G: Nuclear and Particle Physics* 43.8 (2016). ISSN: 13616471. DOI: 10.1088/0954-3899/43/8/084001. arXiv: 1601.07459.

[2] M. G. Aartsen et al. "Evidence for high-energy extraterrestrial neutrinos at the icecube detector". In: *Science* 342.6161 (2013), pp. 1–38. ISSN: 10959203. DOI: 10.1126/science.1242856. arXiv: 1311.5238.

[3] B. P. Abbott et al. "GW150914: Implications for the stochastic gravitational-wave background from binary black holes". In: *Physical Review Letters* 116.13 (2016). ISSN: 10797114. DOI: 10.1103/PhysRevLett.116.131102. arXiv: 1602.03847.

[4] F. Von Feilitzsch and L. Oberauer. "Neutrinos". In: *The Rudolf Mössbauer Story: His Scientific Work and Its Impact on Science and History* 9783642179 (2012), pp. 393–415. ISSN: 2250-6101. DOI: 10.1007/978-3-642-17952-5_20. arXiv: 0103091 [physics].

[5] Q. R. Ahmad et al. "Direct Evidence for Neutrino Flavor Transformation from Neutral-Current Interactions in the Sudbury Neutrino Observatory". In: *Physical Review Letters* 89.1 (2002), pp. 6–11. ISSN: 10797114. DOI: 10.1103/PhysRevLett.89.011301. arXiv: 0204008 [nucl-ex].

[6] M. H. Ahn et al. "Indications of Neutrino Oscillation in a 250 km Long-Baseline Experiment". In: *Physical Review Letters* 90.4 (2003), p. 5. ISSN: 10797114. DOI: 10.1103/PhysRevLett.90.041801. arXiv: 0212007 [hep-ex].

[7] T. Araki et al. "Measurement of neutrino oscillation with KamLAND: Evidence of spectral distortion". In: *Physical Review Letters* 94.8 (2005), pp. 1–5. ISSN: 00319007. DOI: 10.1103/PhysRevLett.94.081801. arXiv: 0406035 [hep-ex].

[8] Y. Fukuda et al. "Evidence for oscillation of atmospheric neutrinos". In: *Physical Review Letters* 81.8 (1998), pp. 1562–1567. ISSN: 10797114. DOI: 10.1103/PhysRevLett.81.1562. arXiv: 9807003 [hep-ex].

[9] V. Barger, D. Marfatia, and K. Whisnant. "Breaking Eight-fold Degeneracies in Neutrino CP Violation, Mixing, and Mass Hierarchy". In: (2001), pp. 1–35. DOI: 10.1103/PhysRevD.65.073023. arXiv: 0112119 [hep-ph]. URL: http://arxiv.org/abs/hep-ph/0112119%7B%5C%%7D0Ahttp://dx.doi.org/10.1103/PhysRevD.65.073023.

[10] Igor Ostrovskiy and Kevin O'Sullivan. "Search for neutrinoless double beta decay". In: *Modern Physics Letters A* 31.18 (2016), pp. 1–21. ISSN: 02177323. DOI: 10.1142/S0217732316300172. arXiv: 1605.00631.

[11] Robert Bormuth. "Chasing cosmic tau neutrinos in the abyss". Doctoral Thesis. Leiden, 2017. URL: http://hdl.handle.net/1887/56023.

[12] Maite Boden. "Time calibration and detector consistency cross checks of the KM3NeT detector using atmospheric particles Time calibration and detector consistency cross checks of the KM3NeT detector using atmospheric particles". Bachelor Thesis. Leiden, 2019.

[13] J. V. Jelley. *The Cerenkov effect and its applications*. 1958, p. 303.

[14] Donald E. Groom, Nikolai V. Mokhov, and Sergei I. Striganov. "Muon stopping power and range tables 10 MeV-100 TeV". In: *Atomic Data and Nuclear Data Tables* 78.2 (2001), pp. 183–356. ISSN: 0092640X. DOI: 10.1006/adnd.2001.0861.

[15] T. Chiarusi and M. Spurio. "High-Energy Astrophysics with Neutrino Telescopes". In: (2009), pp. 1–89. DOI: 10.1140/epjc/s10052-009-1230-9. arXiv: 0906.2634. URL: http://arxiv.org/abs/0906.2634%7B%5C%%7D0Ahttp://dx.doi.org/10.1140/epjc/s10052-009-1230-9.

[16] KM3NeT Collaboration et al. "Dependence of atmospheric muon rate on seawater depth measured with the first KM3NeT detection units". In: (2019). arXiv: 1906.02704. URL: http://arxiv.org/abs/1906.02704.

[17] Rosa Coniglione. *Collaboration communication*. 2018. URL: https://elog.km3net.de/Analysis/286.